Supporting Information

Stabilizing Lithium Metal Anode with Bismuth Oxide-Coated 3D Copper Foam via an In-Situ Bifunctional Mediation Layer

Yida Wang [a], Juntao Si [a], Yiran Zhu [a], Kuo Cao [a], Sihan Zeng [a], Yunyong Hu [a], Bicai Pan [b, c], Chunhua Chen [a *]

[a] Chinese Academy of Sciences Key Laboratory of Precision and Intelligent Chemistry, Department of Materials Science and Engineering, University of Science and Technology of China, Hefei 230026, Anhui, China

[b] Hefei National Laboratory for Physical Sciences at the Micro Scale, University of Science and Technology of China, Hefei, Anhui 230026, China

[c] Key Laboratory of Strongly Coupled Quantum Matter Physics, Department of Physics, University of Science and Technology of China, Hefei, Anhui 230026, China

[*] Corresponding author: E-mail address: cchchen@ustc.edu.cn

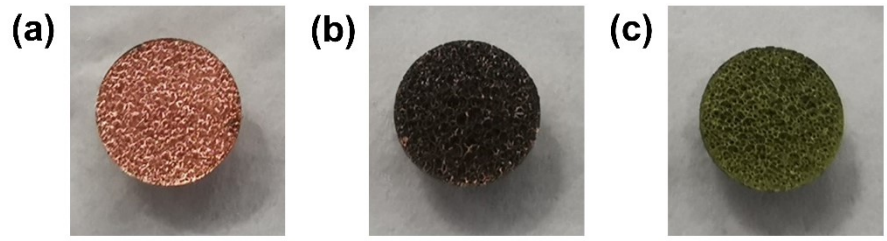

Fig. S1. Digital images of (a) Cu foam, (b) Bi@CF and (c) BO@CF.

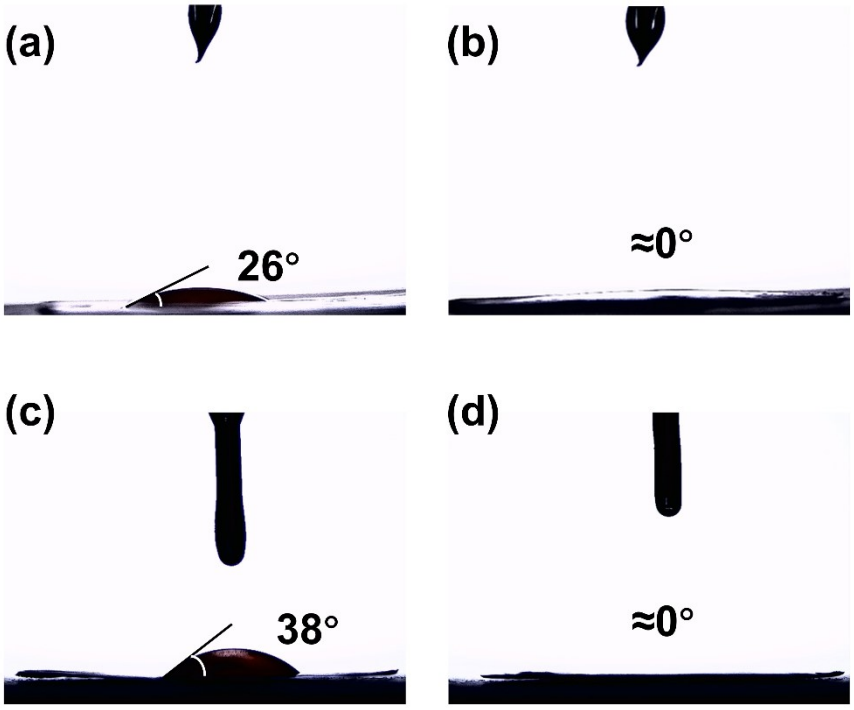

Fig. S2. Contact angles of ether electrolyte (1.0 M LiTFSI in 1,3-dioxolane (DOL)/dimethoxyethane (DME), 1:1 v/v, with 2.0% $LiNO_3$) on the surface of the (a) Cu foil and (b) BO@Cu foil, and ester electrolyte (1.0 M $LiPF_6$ in ethylene carbonate (EC)/dimethyl carbonate (DMC), 1:1 v/v) on the surface of the (c) Cu foil and (d) BO@Cu foil.

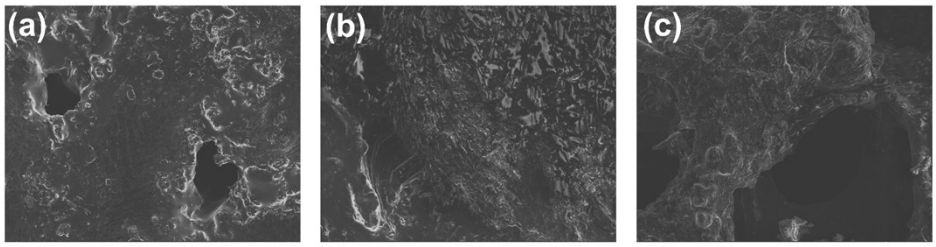

Fig. S3. Schematic illustration of Li plating/stripping mechanisms on Bi@CF current collectors. SEM images with different Li plating capacities of (a) 5 mAh cm^{-2}, (b) 10 mAh cm^{-2}, and (c) followed by stripping 10 mAh cm^{-2} to 50 mV.

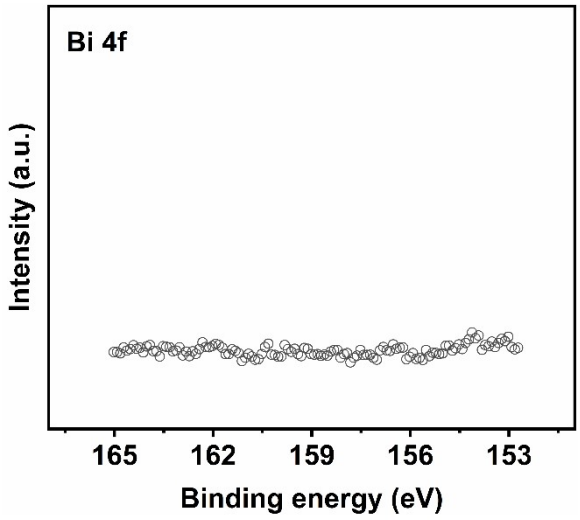

Fig. S4. The XPS of Bi 4f on the lithiated BO@CF surface without e-beam etching.

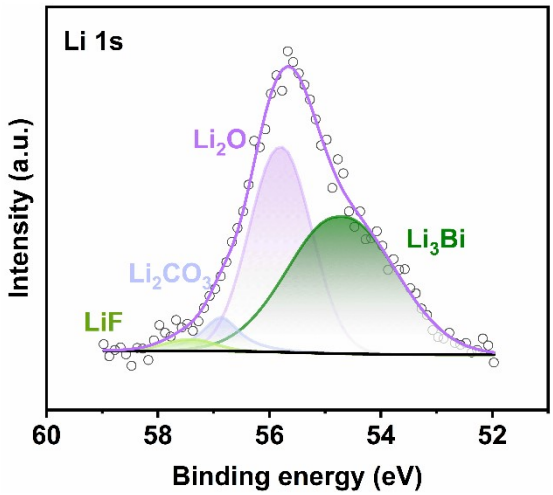

Fig. S5. The XPS of Li 1s on the lithiated BO@CF surface with e-beam etching.

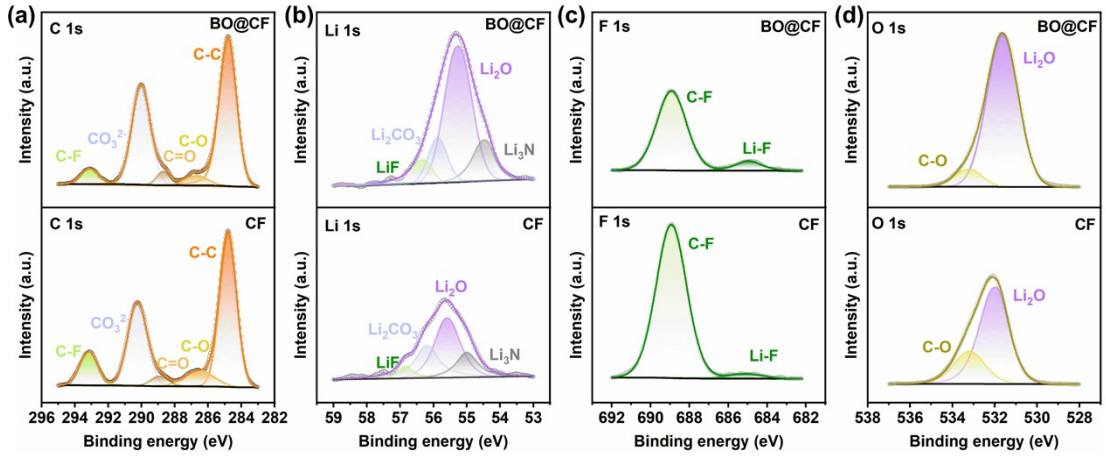

Fig. S6. XPS spectra for BO@CF and CF of C 1s (a), Li 1s (b), F 1s (c) and O 1s (d) after 50 cycles.

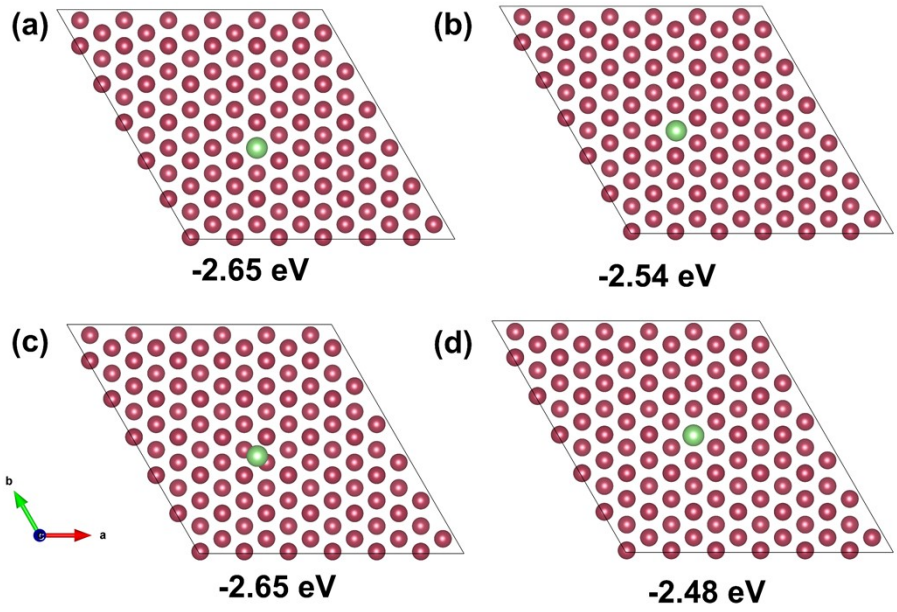

Fig. S7. The adsorption sites and the corresponding adsorption energies of Li on the surface of Cu (111).

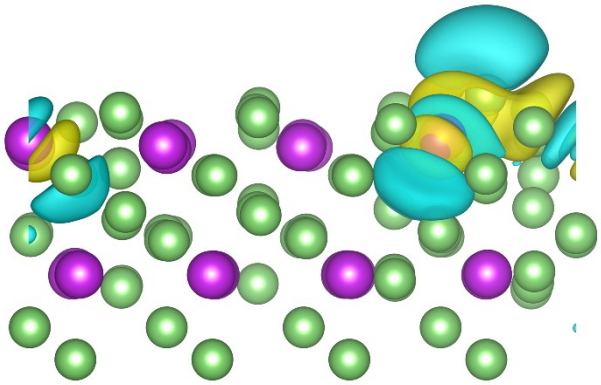

Fig. S8. Electron density differences of Li on the Li_3Bi (111) surface.

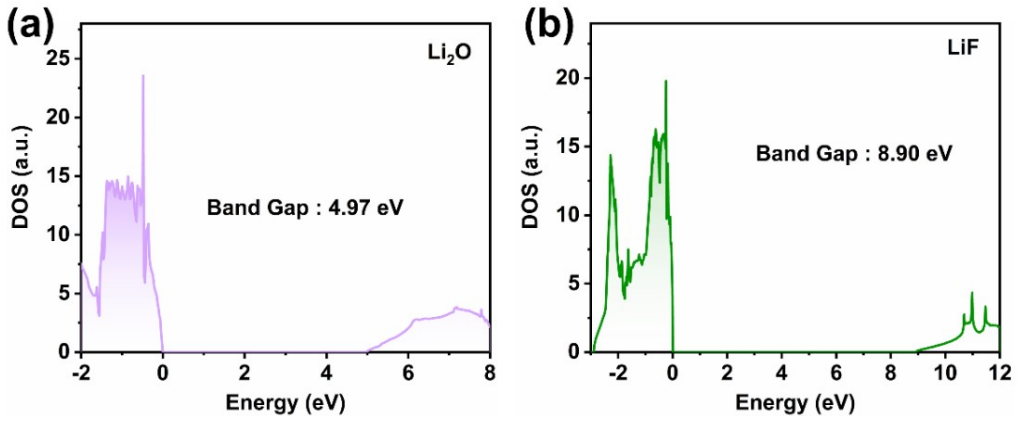

Fig. S9. The DOS of (a) Li_2O and (b) LiF.

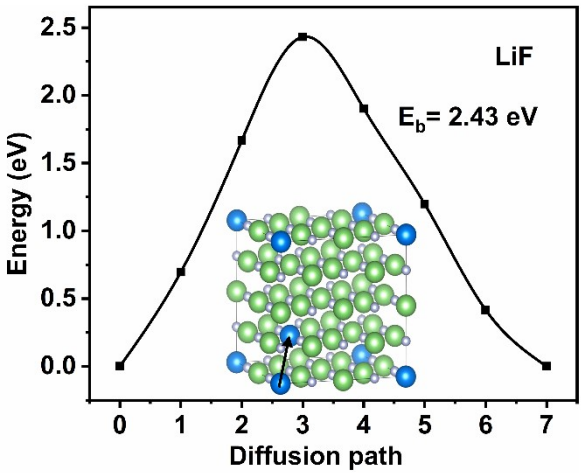

Fig. S10. The diffusion energy barrier of Li in bulk LiF along the $[2\bar{1}1]$ direction.

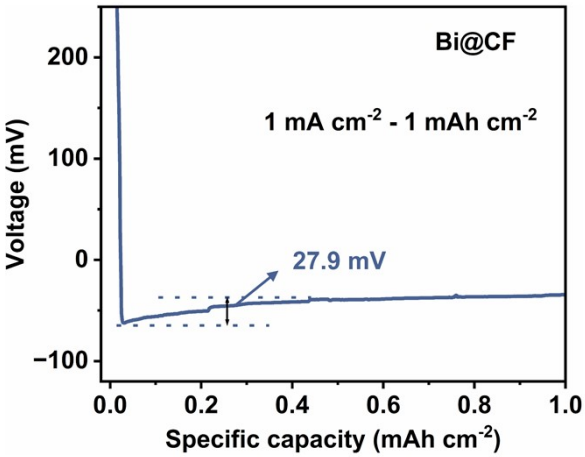

Fig. S11. Nucleation overpotentials of Bi@CF at 1 mA cm^{-2}.

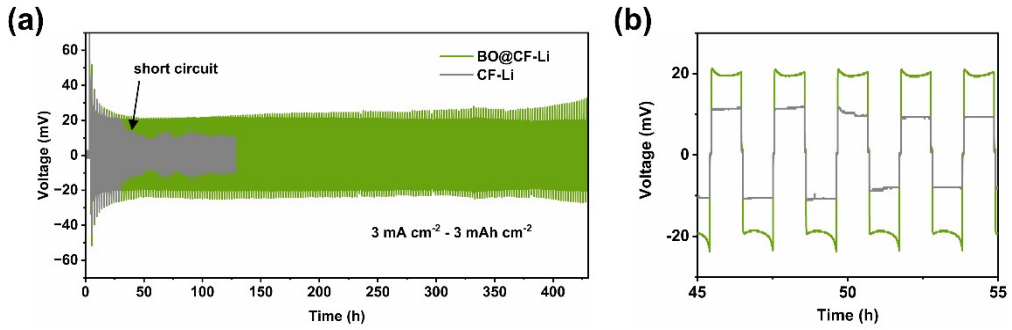

Fig. S12. Voltage curves of Li||Li symmetrical cells at a current density of 3 mA cm^{-2} with a cycling capacity of 3 mAh cm^{-2}. (b) Enlarged view of the short-circuit section.

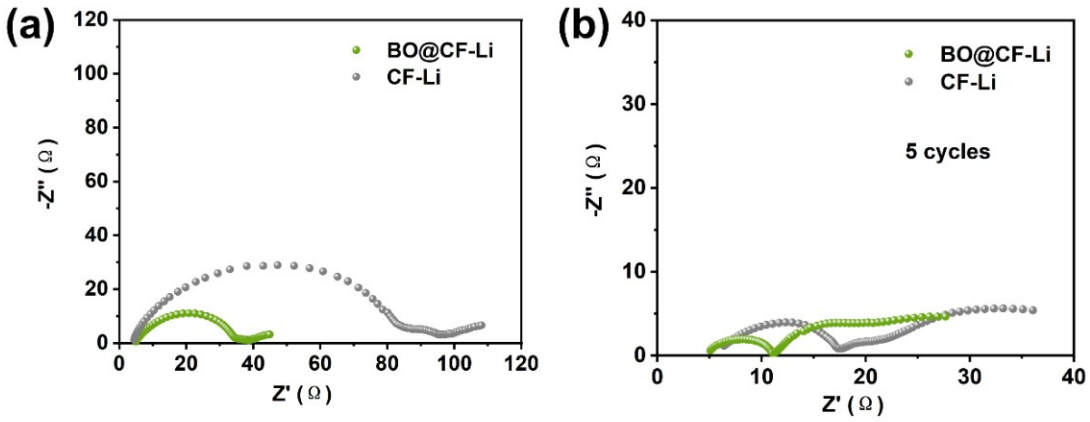

Fig. S13. EIS plot for BO@CF-Li and CF-Li symmetrical cells (a) before and (b) after cycling.

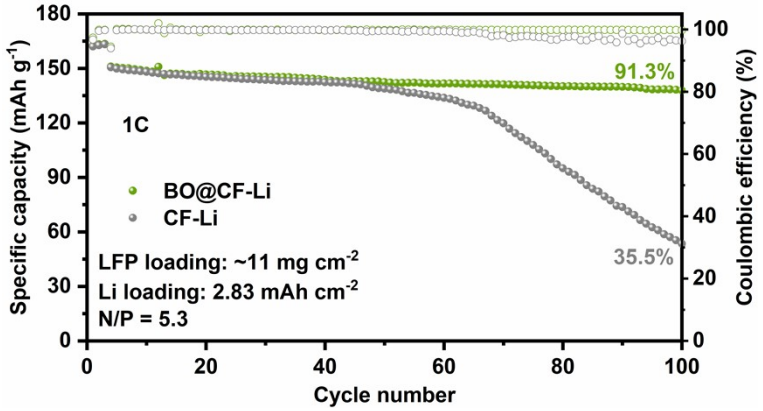

Fig. S14. Cycling performances of LFP||BO@CF-Li and LFP||CF-Li full cells at a rate of 1 C under the N/P ratio of 1.5.

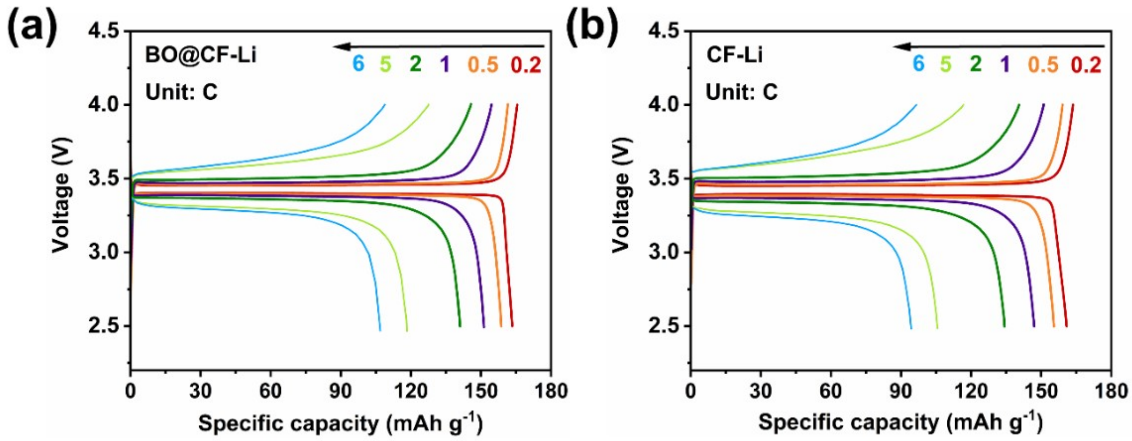

Fig. S15. The charge/discharge curves of the first cycle at different rates for full cells of (a) BO@CF-Li||LFP, (b) CF-Li||LFP.

Table S1. The comparison of cycling performance of half cells with BO@CF and other modified copper foams previously reported in literature. The electrolytes used are all 1 M LiTFSI in 1:1(v/v) DOL/DME with 1~4% $LiNO_3$. (Note: Cycle life here is the number of cycles at which the coulombic efficiency begins to continuously decay. The cycle life of 180 cycles for Bi@CF in ref. [1] refers only to the maximum life data given in the paper.)

Current collector	Cycle number	Over potential (mV)	Ref.
Sb-NW@CF	140	32.6	[14]
Bi@CF	180	32	[1]
Sb@CF	500	53.8	[21]
Ag@CF	490	36.8	[38]
Sn-Cu_2O@CF	150	60.5	[39]
NiO@CF	320	23	[40]
CuFePBA@CF	300	26	[41]
ZnO@CF	300	35	[42]
BO@CF	**600**	**13.9**	**This work**

Table S2. The initial coulombic efficiency (ICE) and the average coulombic efficiency (ACE) of BO@CF-Li||LFP, CF-Li||LFP and Cufoil-Li||LFP.

	BO@CF-Li||LFP	CF-Li||LFP	Cufoil-Li||LFP
ICE	94.51%	93.96%	96.10%
ACE (100 cycles)	99.84%	98.60%	99.11%